Journal of Shipping and Ocean Engineering 15 (2021) 8-28

Doi: 10.17265/2159-5879/2025.01.002



Vibro-acuostic Analysis of Muti-Stepped Circular Cylindrical Shells Immersed in Fluid Medium

Kwanghun Kim¹, Hyongsik Hong², and Songchol Jo¹

- 1. Mechanical Engineering Faculty No.1, Pyongyang University of Mechanical Engineering, Democratic People's Republic of Korea
- 2. Institute of Mechanics, State Academy of Science, Democratic People's Republic of Korea

Abstract: In this paper, a semi-analytical method for investigating the vibro-acoustic characteristics of multi-stepped cylindrical shells (MSCS) immersed in infinite fluid medium is presented. Based on the Flugge's thin shell theory, the theoretical model for vibration analysis of MSCS is established, whereas acoustic analysis is carried out by employing the Kirchhoff–Helmholtz integral equation. The Chebyshev polynomials is set as shape function for vibro-acoustic analysis of the MSCS, all displacement components are expressed by the Chebyshev polynomials in meridional direction and Fourier series in circumferential direction. For discretizing of acoustic boundary, a set of Chebyshev collocation points and spectral boundary element are introduced, and for solving the non-uniqueness problem in acoustic analysis, the CHIEF method is applied. Through comparison studies with the results of previous literature and the coupled finite element method/ boundary element method (FEM/BEM), the accuracy, convergence and reliability of the proposed method are verified. Finally, the effects of geometry, boundary conditions, fluid medium, material properties and type of applied force on the vibro-acoustic characteristics of MSCS are investigated by several numerical examples.

Key words: MSCS, acoustic medium, vibration analysis, sound radiation, vibro-acoustic analysis

1. Introduction

It is well known that circular cylindrical shells are the main components widely used in the fields of mechanical engineering, aerospace, shipbuilding, chemical industry, etc. A detailed example is the fuselage of a carrier-rocket or space vehicle in the aerospace industry, the fuselage of a submarine in the shipping industry, and the pressure vessels in the chemical industry. These structures, especially those used in airframe or ship fuselage, are operated under various working conditions and environments, and can cause vibrations and noise during the operation. Since the vibration and noise generated during the operation have detrimental effects on the life, strength and health of the machine, the study of accurately analyzing and predicting the vibro-acoustic characteristics is being carried out.

Based on the hypothesis of Kirchhoff-Love, thin shell theories such as Flügge's theory,

Corresponding author: Hyonsik Hong, Dr.; E-mail: hyonsik-hong@star-co.net.kp.

Reissner-Naghdi's theory, Goldenveizer-Novozhilov's were developed for the dynamic characterization of shell structures [1, 2]. With the development of shell theory, extensive research has been carried out to develop high-accuracy and efficient calculation methods. In this process, many efficient solution methods have been proposed, such as general domain decomposition methods [3, 4], the Ritz method [5-9], differential quadrature method [10-13], FEM [14-16], wave propagation approach [17, 18], Galerkin method [19, 20], meshless method [21-23], the dynamics stiffness method [24-26] discrete singular solution method [27, 28], and Haar wavelet method [29]. Depending on the working conditions and structural requirements, in some cases a stepped cylindrical shell structure is required, and the study to analyze the dynamic characteristics of a stepped cylindrical shell is carried out in Refs [30-32].

Much research has been done on the analysis of sound radiation problem of elastic structures in fluid medium as well as on the analysis of vibration of

cylindrical shells. The most widely used method for the analysis of sound radiation problem of elastic structures immersed in a fluid medium is the coupled FEM/BEM. In this method, FEM is used to describe the dynamic behavior of the structure, and BEM is used to represent the acoustic load acting on the structure. The continuity condition at the interface between the structure and fluid is that the normal velocity and the continuity of the sound pressure acting on the surface of the structure must be ensured. While FEM has advantages in structural dynamic behavior analysis, BEM has advantages in acoustic analysis, where all discretization and numerical approximations are located on the surface of the structure. Moreover, the radiation condition exiting infinity is automatically satisfied in BEM [33] when the fluid medium exists in an infinite space. The accurate results may be obtained by discretizing the shell and fluid medium boundaries using two- or three-dimensional finite elements and two-dimensional boundary elements [34-38]. Denli and Sun [39] used two-dimensional finite elements and two-dimensional boundary elements for acoustic analysis both inside and outside of sandwich cylindrical shells. Bérot and Peseux [40] presented an analytical formulation and numerical meodel to investigate the vibro-acoustic behavior of submerged cylindrical shells immersed in heavy fluid. To investigate the vibration and acoustic responses of a submarine hull under harmonic excitation, Caresta et al. [41, 42] used the power series-wave solution. By using the double reflection method, Chen et al. [43] investigated vibro-acoustic behavior of cylindrical shell with complex acoustic boundary conditions. Based on a general higher-order shear deformable zig-zag theory, Qu et al. [44] presented a semi-analytical approach obtaining for vibro-acoustic characteristics of multilayered shell such as cylindrical, conical and spherical shell immersed in a light or heavy fluid. Zou et al. [45] presented an analytical formulation for the underwater acoustic radiation of a cylindrical shell with an internal flexural floor based on the reciprocity theorem, Liu et al. [46] investigated vibration behavior and acoustic radiation of a finite cylindrical shell partially covered with circumferential compliant layers by using the method presented in Ref. [45]. Wang et al. [47] presented an analytical model of vibro-acoustic response of a stiffened submerged cylindrical shell with force and acoustic excitation, the accuracy of the model was verified experimentally.

When acoustic analysis is performed based on the classical Kirchhoff-Helmholtz integral equation, it is possible that the boundary element is either two-dimensional or one-dimensional, and therefore may not give a unique solution at some fictitious frequencies [48]. These frequencies have no physical meaning and produce insignificant peaks in the acoustic response, which can be effectively removed using the CHIEF method [49] or Burton-Miller method [50]. In addition to the study of the vibro-acoustic analysis of various types of individual vibro-acoustic shells. the analysis interconnected structure of shells such as conical, cylindrical and spherical shapes has also been studied [51-56].

As can be seen from the previous work, there has been a lot of work on vibro-acoustic analysis of shells with uniform thickness, whereas no research on vibro-acoustic analysis of stepped shells has been found. Therefore, the present paper focuses on the analysis of the vibro-acoustic properties of MSCS immersed in an infinite fluid medium. Based on the Flügge's thin shell theory, the theoretical formulation for the vibration analysis of a MSCS is established, the variational principles is adopted. Acoustic analysis of MSCS is carried out by employing the Kirchhoff-Helmholtz integral equation, for solving the non-uniqueness problem in acoustic analysis, the method is applied. CHIEF The Chebyshev polynomials is set as shape function for vibro-acoustic analysis of the MSCS, all displacement components are expressed by the Chebyshev polynomials in meridional direction and Fourier series in circumferential direction. Vibro-acoustic response of the MSCS with material properties under various boundary conditions are presented through numerical examples.

2. Theoretical Formulation

2.1 Description of the Model

The geometric model of MSCS is shown in Fig. 1. The MSCS consists of N uniform shells of length L_i ,

thickness h_i and middle surface radius is R. Subscript i(1, 2, ..., N) denotes number of step. A cylindrical shell of uniform thickness can be obtained by setting the thickness of individual steps equal. The cylindrical shell is defined by an orthogonal coordinate system (x, θ, z) with x in the horizontal direction, θ in the circumferential direction, and z in the normal direction of middle surface MSCS. The displacements components in the x, θ and z directions of individual shells are expressed by u_i , v_i and w_i , respectively.

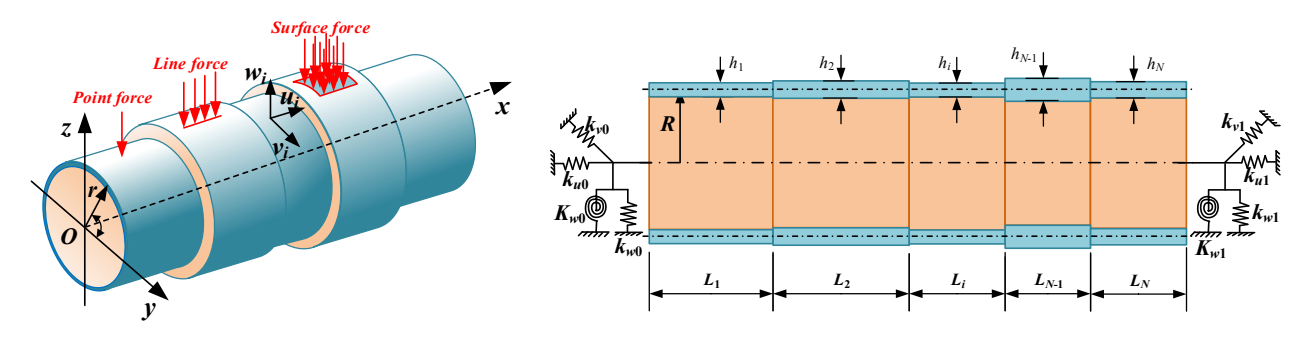


Fig. 1 Geometry and coordinate system of a MSCS.

2.2 Vibration Analysis Model

According to Flügge's thin shell theory, the linear strain expressions are defined as following [1, 2].

$$\varepsilon_{x}^{i} = \varepsilon_{x,0}^{i} + z_{i} \chi_{x}^{i}, \qquad \varepsilon_{\theta}^{i} = \frac{1}{1 + z_{i} / R} \left(\varepsilon_{\theta,0}^{i} + z_{i} \chi_{\theta}^{i} \right),$$

$$\gamma_{x\theta}^{i} = \frac{1}{1 + z_{i} / R} \left[\gamma_{x\theta,0}^{i} + \left(1 + \frac{z_{i}}{2R} \right) \chi_{x\theta}^{i} \right]$$

$$(1)$$

In Eq. (1), $\varepsilon_{x,0}^i$, $\varepsilon_{\theta,0}^i$ and $\gamma_{x\theta,0}^i$ denote the normal and shear strains in the middle surface of the i^{th} step shell, χ_x^i , χ_θ^i and $\chi_{x\theta}^i$ denote the curvature and twist deformations.

They are written as follows:

$$\varepsilon_{x,0}^{i} = \frac{\partial u_{0}^{i}}{\partial x}, \quad \varepsilon_{\theta,0}^{i} = \frac{\partial v_{0}^{i}}{R \partial \theta} + \frac{w_{0}^{i}}{R}, \quad \gamma_{x\theta,0}^{i} = \frac{\partial v_{0}^{i}}{\partial x} + \frac{\partial u_{0}^{i}}{R \partial \theta}$$

$$\chi_{x}^{i} = -\frac{\partial^{2} w_{0}^{i}}{\partial x^{2}}, \quad \chi_{\theta}^{i} = \frac{\partial v_{0}^{i}}{R^{2} \partial \theta} - \frac{\partial^{2} w_{0}^{i}}{R^{2} \partial \theta^{2}}, \quad \chi_{x\theta}^{i} = \frac{\partial v_{0}^{i}}{R \partial x} - 2\frac{\partial^{2} w_{0}^{i}}{R \partial x \partial \theta}$$
(2)

According to Hooke's law on stress-strain relationship, the corresponding stresses components of individual step shell can be expressed as follows:

$$\begin{Bmatrix} \sigma_{x}^{i} \\ \sigma_{\theta}^{i} \\ \tau_{x\theta}^{i} \end{Bmatrix} = \begin{bmatrix} \frac{E}{1-\mu^{2}} & \frac{\mu E}{1-\mu^{2}} & 0 \\ \frac{\mu E}{1-\mu^{2}} & \frac{E}{1-\mu^{2}} & 0 \\ 0 & 0 & \frac{E}{2(1+\mu)} \end{bmatrix} \begin{bmatrix} \varepsilon_{x}^{i} \\ \varepsilon_{\theta}^{i} \\ \gamma_{x\theta}^{i} \end{bmatrix} (3)$$

where E and μ are Young's modulus and Poisson's ratio, respectively.

From the elastic theory, the strain energy function in the i^{th} step shell can be expressed as

$$U_{s}^{i} = \frac{1}{2} \iiint_{V} \left[\sigma_{x}^{i} \varepsilon_{x}^{i} + \sigma_{\theta}^{i} \varepsilon_{\theta}^{i} + \tau_{x\theta}^{i} \gamma_{x\theta}^{i} \right] R dx d\theta dz$$

$$= \frac{Eh_{i}}{2(1-\mu^{2})} \int_{x} \int_{\theta} \left\{ \left(\varepsilon_{x,0}^{i}\right)^{2} + \left(\varepsilon_{\theta,0}^{i}\right)^{2} + 2\mu\varepsilon_{x,0}^{i}\varepsilon_{\theta,0}^{i} + \frac{1-\mu}{2}\left(\tau_{x\theta,0}^{i}\right)^{2} + \frac{1-\mu}{2}\left(\tau_{x\theta,0}^{i}\right)^{2} + \frac{h^{2}}{12} \left[\left(\chi_{x}^{i}\right)^{2} + \left(\chi_{\theta}^{i}\right)^{2} + 2\mu\chi_{x}^{i}\chi_{\theta}^{i} + \frac{1-\mu}{2}\left(\chi_{\theta}^{i}\right)^{2} + \frac{1-\mu}{2R}\gamma_{x\theta,0}^{i}\chi_{\theta}^{i} + \left(\frac{\varepsilon_{\theta,0}^{i}}{R}\right)^{2} + \frac{1-\mu}{2R^{2}}\gamma_{x\theta,0}^{i}\right] \right\} Rdxd\theta$$

$$(4)$$

The kinetic energy of i^{th} step shell can be written as:

$$T^{i} = \frac{\rho h}{2} \iint_{\mathcal{X}} \left[\left(\dot{u}_{i} \right)^{2} + \left(\dot{v}_{i} \right)^{2} + \left(\dot{w}_{i} \right)^{2} \right] R dx d\theta$$
 (5)

The effect of external loads to study the force vibration characteristic of proposed structure can be expressed as following energy function [32].

$$W^{i} = \iint_{\mathcal{X}} \left(f_{u} u_{0}^{i} + f_{v} v_{0}^{i} + f_{w} w_{0}^{i} \right) R d\theta dx \qquad (6)$$

where, f_u , f_v and f_w are the external forces in the meridional, circumferential, and the normal directions, respectively.

The virtual work corresponding to the external acoustic medium pressure can be expressed as follows.

$$W_f^{\xi} = - \iint_{\mathbf{r}} w_i(\overline{\mathbf{r}}) \, \overline{p}_i(\overline{\mathbf{r}}) \, dx d\theta \tag{7}$$

Where p_i is the acoustic medium pressure acting on the ith step shell.

By applying the pseudo-stiffness technique, the boundary and continuity conditions can be generalized, and the potential energy stored in the boundary and connecting springs are given as follows, respectively.

In Eq. (8) symbols k_u , k_v , k_w and K_w are the boundary spring stiffness. Table 1 shows the spring stiffness value corresponding to the several boundary conditions.

$$U_{B} = \int_{\theta} \left\{ \begin{bmatrix} k_{u0}u^{2} + k_{v0}v^{2} + k_{w0}w^{2} + K_{w0}(\partial w / \partial x) \end{bmatrix}_{x=0} + \left[k_{u1}u^{2} + k_{v1}v^{2} + k_{w1}w^{2} + K_{w1}(\partial w / \partial x) \right]_{x=L} \right\} R d\theta$$
 (8)

Table 1 The spring stiffness value corresponding to the boundary conditions.

BC	$k_{u,0}, k_{u,1}$	$k_{v,0}, k_{v,1}$	$k_{w,0}, k_{w,1}$	$k_{arphi,0},k_{arphi,1}$	$k_{ heta,0},k_{ heta,1}$	
F	0	0	0	0	0	
SD	0	10^{14}	10^{14}	0	0	
SS	10^{14}	10^{14}	10^{14}	0	10^{14}	
C	10^{14}	10^{14}	10^{14}	10^{14}	10^{14}	
E_{1}	10^{8}	10^{8}	10^{8}	10^{14}	10^{14}	
E_2	10^{14}	10^{14}	10^{14}	10^{8}	10^{8}	
E ₃	10^{8}	10^{8}	10^{8}	10^{8}	10^{8}	

$$U_{C} = \int_{\theta} \left\{ k_{uc} \left(u_{i} - u_{i+1} \right)^{2} + k_{vc} \left(v_{i} - v_{i+1} \right)^{2} + k_{wc} \left(w_{i} - w_{i+1} \right)^{2} \right\} R d\theta$$

$$\left\{ + K_{wc} \left[\left(u_{i} - \partial w_{i} / \partial x \right) - \left(u_{i+1} - \partial w_{i+1} / \partial x \right) \right] \right\} R d\theta$$
(9)

In addition, in Eq. (9), k_{uc} , k_{vc} , k_{wc} and K_{wc} represent the connection spring stiffness. By setting the stiffness value of the connecting spring to infinity (10¹⁴), the individual shells can be considered as rigid bonded shells.

In this paper, the displacement is parametrically represented by the Chebyshev polynomial of first kind in the meridional direction and Fourier series in the circumferential direction, can be written as follows:

$$u_0^i(x,\theta,t) = \sum_{m=0}^M \sum_{n=0}^N T_m(\phi) \left[\bar{U}_{mn}^i \cos(n\theta) + \tilde{U}_{mn}^i \sin(n\theta) \right] e^{i\omega t}$$
(10a)

$$v_0^i(x,\theta,t) = \sum_{m=0}^M \sum_{n=0}^N T_m(\phi) \left[\bar{V}_{mn}^i \sin(n\theta) + \tilde{V}_{mn}^i \cos(n\theta) \right] e^{i\omega t}$$
(10b)

$$w_0^i(x,\theta,t) = \sum_{m=0}^M \sum_{n=0}^N T_m(\phi) \left[\overline{W}_{mn}^i \cos(n\theta) + \widetilde{W}_{mn}^i \sin(n\theta) \right] e^{i\omega t}$$
(10c)

where $T_m(\phi)$ is the m-order Chebyshev polynomial, which means the displacement function in the meridional direction, and the maximum degree is M.

$$\overline{U}_{mn}^i, \widetilde{U}_{mn}^i, \overline{V}_{mn}^i, \widetilde{V}_{mn}^i, \overline{W}_{mn}^i$$
 and \widetilde{W}_{mn}^i are unknown

coefficients of the polynomial to be determined. ω is an angular frequency, t denotes time. n is the circumferential wave number, and the maximum degree is N.

The m^{th} polynomial of Chebyshev polynomial of first kind uniformly defined as [32].

$$T_m(\phi) = \cos(m \arccos \phi); \ (m = 0, 1, 2, ..., |\phi| \le 1) \ (11)$$

By employing the trigonometric relation $\cos[(m+1)\phi] + \cos[(m-1)\phi] = 2\cos\phi\cos m\phi$, the repetitive equation of the Chebyshev polynomial can be written as:

$$T_{m+1}(\phi) = 2xT_m(\phi) - T_{m-1}(\phi)$$
 (12)

Thus, the Chebyshev polynomials can be obtained as:

$$T_{m+1}(\phi) = \sum_{k=0}^{[m/2]} (-1)^k \frac{m!}{(2k)!(m-2k)!} \phi^{m-2k} (1-\phi^2)^k$$
(13)

where [m/2] denotes the integer part of m/2.

The Chebyshev polynomial are complete and orthogonal polynomials defined on the interval of $\phi \in [-1,1]$. Thus, a linear transformation statute must be introduced for coordinate conversion from interval $x \in [0, L_i]$ of the individual step shell to interval $\phi(\phi \in [-1,1])$ of the Chebyshev polynomial,

Since the Chebyshev polynomial is an orthogonal function defined in the interval $\phi \in [-1,1]$, the actual interval of the individual shell $x \in [0, L_i]$ must be linearly transformed into a polynomial interval. Thus, the following linear transformation condition must be

introduced;
$$\phi = \frac{2}{L_i} x - 1$$
 or $x = \frac{L_i}{2} (\phi + 1)$.

The total Lagrangian energy L of the MSCS can be expressed as:

$$L = \sum_{i=1}^{N} (T^{i} - U_{s}^{i}) - (U_{B} + U_{C}) + (W^{i} + W_{f}^{i})$$
 (14)

According to the Rayleigh-Ritz method, the total Lagrangian energy of the MSCS is minimized by partial derivation with respect to the unknown coefficients.

$$\frac{\partial \mathbf{L}}{\partial \mathcal{A}} = 0, \quad \mathcal{S} = \overline{U}_{mn}^{i}, \widetilde{U}_{mn}^{i}, \overline{V}_{mn}^{i}, \widetilde{V}_{mn}^{i}, \overline{W}_{mn}^{i}, \widetilde{W}_{mn}^{i}, \widetilde{W}_{mn}^{i}$$
(15)

Substituting Eqs.(4)-(14) into Eq. (15), the discretized vibration equation of the MSCS is obtained as matrix form.

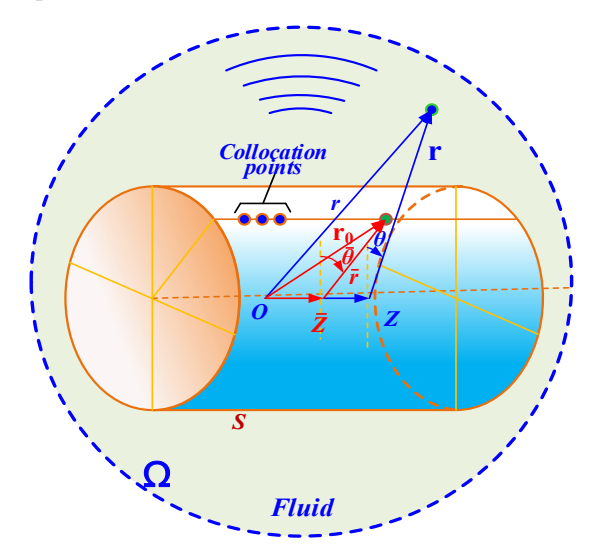
$$\left(\mathbf{K} - \omega^2 \mathbf{M}\right) \mathbf{A} = \mathbf{F}_s + \mathbf{F}_p \tag{16}$$

where **K** and **M** are the stiflfness and mass matrix of the MSCS, and **A** is the coefficient vector, respectively. **F**_S is the generalized force vector due to the external forces acting on the structure, and **F**_P is the force vector generated by the sound pressure of the fluid medium acting on the surface of the shell.

2.3 Acoustic Analysis Model

When sound propagates in a fluid medium due to structural vibrations of an elastic body, some assumptions about the fluid medium are introduced as: (1) A sound-transmitting medium is an ideal fluid that does not take into account the viscosity of the fluid medium and the energy transfer loss of the sound waves in the fluid medium; (2) The initial fluid velocity of the sound-transmitting medium is zero and uniformly distributed; (3) The sound wave transmitted in a fluid medium is an elastic wave with a small amplitude.

In analyzing the acoustic characteristics of structures in fluid-solid coupling space, BEM is a widely applied method due to its ease of coupling with finite element methods, which essentially provides numerical solution of the Helmholtz integral equation. A schematic diagram for considering the problem of external acoustic wave propagation of an axisymmetric elastic structure in sound fields without sound sources and acted forces is shown in Fig. 2.



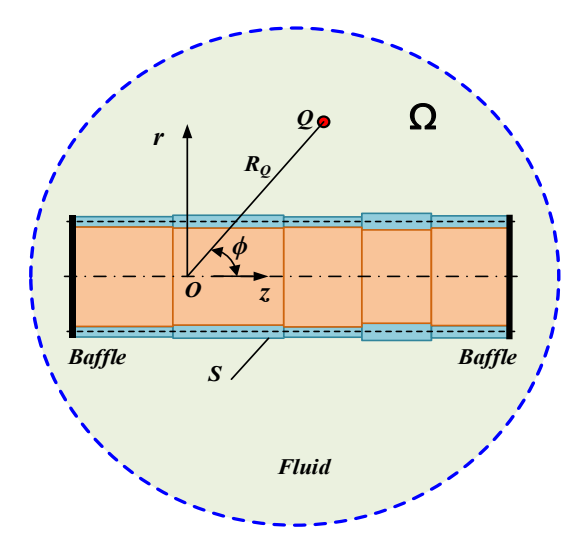


Fig. 2 The coordinate system for analyzing the sound radiation of a MSCS.

Considering that MSCS is axisymmetric, to define the acoustic field, a global coordinate system (r, θ, z) located on the geometric symmetry axis of the MSCS is introduced.

Based on this coordinate system, the Kirchhoff–Helmholtz boundary integral equation governing the exterior sound space of MSCS can be expressed as [56]:

$$C(\mathbf{r})p(\mathbf{r}) = \int_{S} p(\overline{\mathbf{r}}) \frac{\partial G(\mathbf{r}, \overline{\mathbf{r}})}{\partial \overline{n}} - G(\mathbf{r}, \overline{\mathbf{r}}) \frac{\partial p(\mathbf{r}, \overline{\mathbf{r}})}{\partial \overline{n}} ds \quad (17)$$

where $C(\mathbf{r})$ means the position of the point measuring the acoustic characteristics and is defined as:

$$C(\mathbf{r}) = \begin{cases} 1, & \mathbf{r} \in \Omega \\ 0, & \mathbf{r} \notin \Omega, \mathbf{r} \notin S \\ 1/2, & \mathbf{r} \in S \end{cases}$$
(18)

 $\mathbf{r}(r, \theta, z)$ is the radius vector of any measurement point in the sound propagation space Ω and $\mathbf{r}(\overline{r}, \overline{\theta}, \overline{z})$ is the radius vector of any point on the fluid-solid interface \mathbf{S} . $G(\mathbf{r}, \overline{\mathbf{r}})$ is a Green's function and is defined in cylindrical coordinates as follows:

$$G(\mathbf{r}, \overline{\mathbf{r}}) = \frac{e^{-ikR_0(\mathbf{r}, \overline{\mathbf{r}})}}{4\pi R_0(\mathbf{r}, \overline{\mathbf{r}})}$$
(19)

where $k = \omega/c_f$, ω is the vibration frequency, c_f is the velocity of sound in the fluid, and $R_0(\mathbf{r}, \bar{\mathbf{r}})$ is the

distance $R_0(\mathbf{r}, \bar{\mathbf{r}})$ between two vectors \mathbf{r} and $\bar{\mathbf{r}}$ and it is calculated as follows.

$$R_0(\mathbf{r}, \overline{\mathbf{r}}) = \sqrt{r^2 - \overline{r}^2 - 2r\overline{r}\cos(\theta - \overline{\theta}) + (z - \overline{z})^2}$$
 (20)

When analyzing the acoustic behavior of axisymmetric elastic bodies, $P(\mathbf{r})$ and $P(\overline{\mathbf{r}})$ can be expanded into Fourier series in the circumferential direction.

$$p(\mathbf{r}) = \sum_{n=0}^{N} \left[p_n^s(r, n, z) \sin(n\theta) + p_n^c(r, n, z) \cos(n\theta) \right]$$

$$\overline{p}(\overline{\mathbf{r}}) = \sum_{n=0}^{N} \left[\overline{p}_n^s(\overline{r}, \overline{n}, \overline{z}) \sin(n\overline{\theta}) + \overline{p}_n^c(\overline{r}, \overline{n}, \overline{z}) \cos(n\overline{\theta}) \right]$$
(21)

where $p_n^s(r, n, z)$, $p_n^c(r, n, z)$ are the Fourier coefficients of the sound pressure at the measurement point $\mathbf{r}(r, n, z)$ of the sound field, and $\bar{p}_n^s(\bar{r}, \bar{n}, \bar{z})$, $p_n^c(\bar{r}, \bar{n}, \bar{z})$ are the Fourier coefficients of the sound pressure at the interface point $\bar{\mathbf{r}}(\bar{r}, \bar{n}, \bar{z})$ of the sound field (the surface of shell). n is the acoustic

mode number in the circumferential direction. Similarly, expanding the Green's function and its normal derivative into a Fourier series circumferentially at the interface, they can be written as:

$$G(\mathbf{r}, \overline{\mathbf{r}}) = \frac{1}{\pi} \sum_{n=0}^{N} H_n \left[\sin(n\theta) \sin(n\overline{\theta}) + \cos(n\theta) \cos(n\overline{\theta}) \right]$$

$$\frac{\partial G(\mathbf{r}, \overline{\mathbf{r}})}{\partial \overline{n}} = \frac{1}{\pi} \sum_{n=0}^{N} \overline{H}_n \left[\sin(n\theta) \sin(n\overline{\theta}) + \cos(n\theta) \cos(n\overline{\theta}) \right]$$
(22)

In Eq. (22),

$$H_n = \int_0^{2\pi} \frac{e^{-ikR_p}}{4\pi R_0} \cos(n\phi) d\phi, \qquad \bar{H}_n = \int_0^{2\pi} \frac{\partial}{\partial \bar{n}} \left(\frac{e^{-ikR_p}}{4\pi R_0}\right) \cos(n\phi) d\phi \tag{23}$$

The contact surface interaction of the fluid with the body structure can be written as

$$w_i(\overline{\mathbf{r}}) = \frac{1}{\rho_f \omega^2} \frac{\partial \overline{p}(\overline{\mathbf{r}})}{\partial \overline{n}}$$
 (24)

where $w_i(\bar{\mathbf{r}})$ is the normal displacement of the elastic

body at the surface of the elastic body and $\frac{\partial \overline{p}(\overline{\mathbf{r}})}{\partial \overline{n}}$ is

the normal derivative of the sound pressure at the

boundary point of the sound field (the surface of the elastic body).

Substituting Eqs. (21-24) into Eq. (17) and after performing certain algebraic operations, we can obtain the modified form of the Kirchhoff-Helmholtz integral equation as follows [39]:

$$C(\mathbf{r}) \sum_{n=0}^{\tilde{N}} \left[p_n^s (r, n, z) \sin n\theta + p_n^c (r, n, z) \cos n\theta \right] =$$

$$= \int_{I} \left\{ \sum_{n=0}^{\tilde{N}} \left[\overline{p}_n^s (\overline{r}, n, \overline{z}) \overline{H}_n \sin n\theta \right] + \sum_{n=0}^{\tilde{N}} \left[\overline{p}_n^c (\overline{r}, n, \overline{z}) \overline{H}_n \cos n\theta \right] \right\} \overline{r} dl$$

$$- \rho_f \omega^2 \sum_{n=0}^{\tilde{N}} \left[\overline{w}_n^s (\overline{r}, n, \overline{z}) H_n \sin n\theta \right] - \rho_f \omega^2 \sum_{n=0}^{\tilde{N}} \left[\overline{w}_n^c (\overline{r}, n, \overline{z}) H_n \cos n\theta \right] \right\} \overline{r} dl$$
(25)

Eq. (26) can be written simply as

$$C(\mathbf{r}) p_n^s = \int_{l} (\bar{H}_n \bar{p}_n^s - \rho_f \omega^2 H_n w_n^s) \bar{r} dl$$

$$C(\mathbf{r}) p_n^c = \int_{l} (\bar{H}_n \bar{p}_n^c - \rho_f \omega^2 H_n w_n^c) \bar{r} dl$$
(26)

To construct the coupling matrix of solid-fluid interactions, the acoustic boundary *l* must be discretized in such a way that the acoustic boundary segments and shell segments are matched. The sound pressure for each shell segment is expanded as follows:

$$\bar{p}_{n}^{s} = \sum_{j=0}^{J} T_{j}(\xi) \bar{p}_{n,j}^{s} = \mathbf{T}_{p}(\xi) \bar{\mathbf{p}}_{n}^{s}
\bar{p}_{n}^{c} = \sum_{j=0}^{J} T_{j}(\xi) \bar{p}_{n,j}^{c} = \mathbf{T}_{p}(\xi) \bar{\mathbf{p}}_{n}^{c}$$
(27)

where, $T_j(\xi)$ is the j^{th} order Chebyshev orthogonal polynomials of the first kind. $\bar{p}_{n,j}^s$ and $\bar{p}_{n,j}^c$ denote the generalized pressure. Substituting Eqs. (27) and (10c) into Eq. (26), the discretized Kirchhoff-Helmholtz boundary integral equation can be written as following.

$$C(\mathbf{r})\mathbf{J}_{p}(\xi)\overline{\mathbf{p}}_{n}^{s}(\mathbf{r}) = \sum_{i=1}^{N} \int_{l_{i}} \left[H_{n}\mathbf{J}_{p}(\xi)\overline{r}(\xi)|J_{\xi}|\right] d\xi \overline{\mathbf{p}}_{n}^{s}(\overline{\mathbf{r}}) - \rho_{f}\omega^{2} \sum_{i=1}^{N} \int_{l_{i}} \left[H_{n}\mathbf{J}_{\omega}(\xi)\overline{r}(\xi)|J_{\xi}|\right] d\xi \mathbf{W}_{n}^{s}(\overline{\mathbf{r}})$$

$$C(\mathbf{r})\mathbf{J}_{p}(\xi)\overline{\mathbf{p}}_{n}^{c}(\mathbf{r}) = \sum_{i=1}^{N} \int_{I_{i}} \left[H_{n}\mathbf{J}_{p}(\xi)\overline{r}(\xi)|J_{\xi}|\right] d\xi \overline{\mathbf{p}}_{n}^{c}(\overline{\mathbf{r}}) - \rho_{f}\omega^{2} \sum_{i=1}^{N} \int_{I_{i}} \left[H_{n}\mathbf{J}_{\omega}(\xi)\overline{r}(\xi)|J_{\xi}|\right] d\xi \mathbf{W}_{n}^{c}(\overline{\mathbf{r}}) (28)$$

where $\left|J_{\xi}\right|$ is the Jacobian coordinate transformation.

To discretize the boundary integral equation, J+1 collocation points are defined within the boundary element. Such collocation points can be chosen as zero points of orthogonal polynomials. The formula for calculating the zero points of the Chebyshev orthogonal polynomials of the first kind is as:

$$\xi_{j,k} = \cos\left(\frac{2k-1}{2j}\pi\right), \quad k = 1, 2, ..., J+1, j = J+1 \quad (29)$$

By moving the measurement point \mathbf{r} of the sound field to the j^{th} collocation point of the k^{th} boundary element according to the BEM, Eq. (28) can be written as

$$-C\mathbf{J}_{p}\left(\xi_{k}\right)\overline{\mathbf{p}}_{n,k}^{s}\left(\xi_{k}\right)+\sum_{i=1}^{N}\mathbf{H}_{n,i}\overline{\mathbf{p}}_{n,i}^{s}=\sum_{i=1}^{N}\mathbf{G}_{n,i}\mathbf{W}_{n,i}^{s}$$

$$-C\mathbf{J}_{p}\left(\xi_{k}\right)\overline{\mathbf{p}}_{n,k}^{c}\left(\xi_{k}\right)+\sum_{i=1}^{N}\mathbf{H}_{n,i}\overline{\mathbf{p}}_{n,i}^{c}=\sum_{i=1}^{N}\mathbf{G}_{n,i}\mathbf{W}_{n,i}^{c}$$
(30)

where

$$\mathbf{H}_{n,i} = \int_{l_i} \overline{H}_n \mathbf{J}_p(\xi) \overline{r}(\xi) |J_{\xi}| d\xi$$

$$\mathbf{G}_{n,i} = \rho_f \omega^2 \int_{l_i} H_n \mathbf{J}_w(\xi) \overline{r}(\xi) |J_{\xi}| d\xi$$
(31)

In addition, Eq. (30) can be written in one matrix form as follows:

$$\sum_{n=0}^{N} \mathbf{H}_{n} \overline{\mathbf{P}}_{n} = \sum_{n=0}^{N} \mathbf{G}_{n} \mathbf{W}_{n}$$
 (32)

in which

$$\mathbf{H}_{n} = \left[\underbrace{\mathbf{\overline{H}}_{n,1}, ..., \mathbf{\overline{H}}_{n,i}, ..., \mathbf{\overline{H}}_{n,N}}_{\mathbf{P}_{n}^{s}}, \underbrace{\mathbf{\overline{H}}_{n,1}, ..., \mathbf{\overline{H}}_{n,i}, ..., \mathbf{\overline{H}}_{n,N}}_{\mathbf{P}_{n}^{c}} \right] - \delta_{i}^{k} C(\mathbf{r}) \mathbf{J}_{p} \left(\xi_{k} \right)$$

$$\mathbf{G}_{n} = \left[\underbrace{\mathbf{G}_{n,1}, ..., \mathbf{G}_{n,i}, ..., \mathbf{G}_{n,N}}_{\mathbf{w}_{n}^{s}}, \underbrace{\mathbf{G}_{n,1}, ..., \mathbf{G}_{n,i}, ..., \mathbf{G}_{n,N}}_{\mathbf{w}_{n}^{c}} \right]$$

$$\mathbf{\overline{p}}_{n} = \left[\mathbf{\overline{p}}_{n,1}^{s}, ..., \mathbf{\overline{p}}_{n,i}^{s}, ..., \mathbf{\overline{p}}_{n,N}^{s}, \mathbf{\overline{p}}_{n,1}^{c}, ..., \mathbf{\overline{p}}_{n,i}^{c}, ..., \mathbf{\overline{p}}_{n,N}^{c} \right]^{T}$$

$$\mathbf{w}_{n} = \left[\mathbf{w}_{n,1}^{s}, ..., \mathbf{w}_{n,i}^{s}, ..., \mathbf{w}_{n,N}^{s}, \mathbf{w}_{n,1}^{c}, ..., \mathbf{w}_{n,i}^{c}, ..., \mathbf{w}_{n,N}^{c} \right]^{T}$$
(33)

In order to remove the non-uniqueness of Eq. (32), the CHIEF method is applied, in which, Eq. (30) where the collocation points are set outside of the fluid is used as constraint. If the collocation points \mathbf{r}_i are placed outside the fluid, the quantity $C(\mathbf{r})$ becomes zero and Eq. (30) can be rewritten as

$$\sum_{i=1}^{N} \overline{\boldsymbol{H}} \boldsymbol{c}_{n,i} \boldsymbol{p}_{n,i}^{s} = \sum_{i=1}^{N} \boldsymbol{G} \boldsymbol{c}_{n,i} \boldsymbol{w}_{n,i}^{s}$$

$$\sum_{i=1}^{N} \overline{\boldsymbol{H}} \boldsymbol{c}_{n,i} \boldsymbol{p}_{n,i}^{c} = \sum_{i=1}^{N} \boldsymbol{G} \boldsymbol{c}_{n,i} \boldsymbol{w}_{n,i}^{c}$$
(34)

where

$$\bar{\boldsymbol{H}}\boldsymbol{c}_{n,i} = \int_{L} \bar{\boldsymbol{H}}\boldsymbol{c}_{n} \mathbf{J}_{p}(\xi) \bar{\boldsymbol{r}}(\xi) |J_{\xi}| d\xi$$

$$Gc_{n,i} = \rho_f \omega^2 \int_{I_i} Hc_n \mathbf{J}_w(\xi) \overline{r}(\xi) |J_{\xi}| d\xi$$
 (35)

In addition, Eq. (34) can be simplified as follows:

$$\mathbf{H} = \begin{bmatrix} \tilde{\mathbf{H}}_1 & & & & & \\ & \tilde{\mathbf{H}}_2 & & & & \\ & & \ddots & & & \\ & & & \tilde{\mathbf{H}}_n & & \\ & & & & \tilde{\mathbf{H}}_{\tilde{N}} \end{bmatrix}$$

$$\mathbf{Hc}_{n}\mathbf{p}_{n} = \mathbf{Gc}_{n}\mathbf{W}_{n} \tag{36}$$

Therefore, considering the matrix added by the CHIEF method, when the circumferential wavenumber is unity the boundary element matrix is

$$\tilde{\mathbf{H}}_{n}\mathbf{p}_{n} = \tilde{\mathbf{G}}_{n}\mathbf{w}_{n} \tag{36}$$

where

$$\tilde{\mathbf{H}}_{n} = \left[\mathbf{H}_{n}^{T}, \mathbf{H}\mathbf{c}_{n}^{T}\right]^{T}$$

$$\tilde{\mathbf{G}}_{n} = \left[\mathbf{G}_{n}^{T}, \mathbf{G}\mathbf{c}_{n}^{T}\right]^{T}$$
(37)

Considering the circumferential wave number $n = 0 \sim N$, the discretization matrix of the total boundary integral equation is written as

$$\mathbf{Hp} = \mathbf{Gw} \tag{38}$$

where

$$\mathbf{G} = \begin{bmatrix} \tilde{\mathbf{G}}_1 & & & & & \\ & \tilde{\mathbf{G}}_2 & & & & \\ & & \ddots & & & \\ & & & \tilde{\mathbf{G}}_n & & \\ & & & & \ddots & \\ & & & & \tilde{\mathbf{G}}_{\tilde{N}} \end{bmatrix}$$
(39)

When the structure is immersed in a light fluid, the influence of sound radiation by the fluid can be

neglected because the density of the fluid is much smaller than the material density of the structure, therefore, the vibration and sound radiation problems of the structure can be analyzed separately in this case. However, if the structure is immersed in a heavy fluid, the fluid will affect the force acting on the structure, and thus the acoustic radiation cannot be neglected. The acoustic-vibration coupling system of an elastic structure in a fluid has a close relationship between

the sound pressure and the structural vibration, and therefore structural and acoustic problems must be solved simultaneously. The influence of the sound pressure exerted by the structure in the fluid space is considered as the external force of the structure.

$$W_f = \sum_{i=1}^{N} \int_{l_i} u_i^e \left(-p_i \cdot \vec{n}_e \right) dl \qquad (40)$$

$$\delta W_f^n = -\sum_{i=1}^N \delta \left(\mathbf{w}_{n,i}^s \right)^T \left[S_n^\theta \int_{l_i} \mathbf{J}_w^T \mathbf{J}_p dl \right] \times \mathbf{p}_n^s - \sum_{i=1}^N \delta \left(\mathbf{w}_{n,i}^c \right)^T \left[C_n^\theta \int_{l_i} \mathbf{J}_w^T \mathbf{J}_p dl \right] \times \mathbf{p}_n^c = -\delta \left(\mathbf{w}_n \right)^T \mathbf{C}_n \mathbf{p}_n \quad (41)$$

in which

$$S_n^{\theta} = \int_0^{2\pi} \sin^2(n\theta) d\theta, C_n^{\theta} = \int_0^{2\pi} \cos^2(n\theta) d\theta$$
 (42)

There is a relation of $\mathbf{w} = \mathbf{T}\mathbf{A}$ between the normal displacement and the total displacement of the structure, where \mathbf{T} is the transformation matrix.

The external force \mathbf{F}_p due to the sound pressure can be obtained as

$$\mathbf{F}_{p} = \mathbf{T}^{T} \mathbf{C} \mathbf{p} \tag{43}$$

The acoustic-vibration coupling equation of the fluid-elastic structure is follows as:

$$\begin{cases} (-\omega^2 \mathbf{M} + \mathbf{K}) \mathbf{A} + \mathbf{T}^T \mathbf{C} \mathbf{p} = \mathbf{F} \\ \mathbf{G} \mathbf{T} \mathbf{E} - \mathbf{H} \mathbf{p} = 0 \end{cases}$$
(44)

Eq.(44) can be rewritten as matrix form:

$$\begin{bmatrix} -\omega^2 \mathbf{M} + \mathbf{K} & \mathbf{T}^T \mathbf{C} \\ \mathbf{G} \mathbf{T} & -\mathbf{H} \end{bmatrix} \begin{bmatrix} \mathbf{A} \\ \mathbf{p} \end{bmatrix} = \begin{bmatrix} \mathbf{F} \\ 0 \end{bmatrix}$$
 (45)

By solving Eq. (45), the vectors \mathbf{A} , $\overline{\mathbf{p}}$ can be obtained directly, and then the generalized pressure vector $\overline{\mathbf{p}}$ can be calculated and the sound pressure of any position in the fluid space is also obtained.

3. Numerical Results

In this section, the accuracy, convergence and reliability of the method proposed in this paper for the investigate of the vibro-acoustic responses of MSCS are verified by comparison with the results of the previous literature and FEM/BEM, and the influences of several parameters on the vibro-acoustic characteristics are presented by numerical examples. Unless otherwise stated, in all calculations below, the light fluid is considered as air (the sound velocity c_f = 340 m/s and the density ρ_f = 1.225 kg/m³), and the heavy fluid as water (the sound velocity c_f = 1500 m/s and the density ρ_f = 1026 kg/m³).

Since the range of sound pressure and sound power variations is very large, therefore, in acoustic engineering, the sound pressure level (SPL) and sound power level (SWL) defined by the Eq. (46) are usually used, and the units are decibel (dB).

$$SPL = 20\log\left(\frac{P}{P_{\text{Re}f}}\right), SWL = 10\log\left(\frac{W}{W_{\text{Re}f}}\right)$$
 (46)

The reference sound pressure and the reference sound power in Eq. (46) are set as follows for water and air: the reference sound pressure is $P_{Ref} = 2 \times 10^{-5}$ for water and $P_{Ref} = 1 \times 10^{-6}$ for air, respectively: the reference sound power is $W_{Ref} = 1 \times 10^{-12}$ for both water and air.

3.1 Convergence and Validation

Before investigating the vibro-acoustic characteristics of MSCS, the accuracy, convergence and reliability of the present method must be verified. As shown in Eq. (11), the Chebyshev polynomial can be expanded to infinity. However, increasing the

degree of the polynomial can lead to higher computational accuracy, while the computational efficiency may be reduced. Therefore, it is important to determine the reasonable polynomial degree to achieve high computational efficiency with computational accuracy.

Table 2 shows the change of frequency parameter of the MSCS according to the increment of the

polynomial order. As shown in Table 2, the frequency parameter converges to a certain value as the polynomial order increases. But in all cases, when the polynomial order exceeds 15, there is no change in the frequency parameter. Therefore, the polynomial order is selected as M = 15 for all calculations below.

Table 2 Convergence of frequency parameters according to increase the polynomial order.

	Polynomial order									
B.Cs	n	3	5	7	9	11	13	15	Ref. [32]	
C-F	1	0.062512	0.056642	0.056309	0.056082	0.05594	0.055854	0.0558	0.055788	
	2	0.024446	0.020263	0.020189	0.020137	0.020096	0.020067	0.020047	0.020042	
	3	0.012904	0.010692	0.010666	0.010652	0.010641	0.010631	0.010623	0.010622	
	4	0.011038	0.010158	0.010148	0.010144	0.010141	0.010138	0.010135	0.010134	
	5	0.014407	0.014117	0.014114	0.014112	0.014111	0.01411	0.014108	0.014107	
	6	0.020252	0.020143	0.020141	0.020141	0.02014	0.020139	0.020137	0.020135	
	7	0.027597	0.027545	0.027544	0.027544	0.027543	0.027542	0.027539	0.027538	
	8	0.036197	0.036165	0.036165	0.036164	0.036163	0.036161	0.036158	0.036157	
	9	0.045986	0.045961	0.04596	0.045959	0.045958	0.045956	0.045952	0.045952	
	10	0.056942	0.056919	0.056918	0.056917	0.056915	0.056912	0.056907	0.056909	
C-C	1	0.298475	0.201847	0.197243	0.195424	0.194659	0.194297	0.194105	0.194089	
	2	0.290264	0.101632	0.099219	0.098059	0.097442	0.097099	0.096901	0.096886	
	3	0.287499	0.055651	0.054619	0.054164	0.053882	0.0537	0.053581	0.053574	
	4	0.286428	0.034902	0.034379	0.03419	0.034069	0.033983	0.033921	0.033918	
	5	0.286052	0.026392	0.026111	0.026026	0.025975	0.025936	0.025906	0.025906	
	6	0.2861	0.02569	0.025553	0.025516	0.025495	0.025479	0.025467	0.025468	
	7	0.286522	0.030073	0.030012	0.029995	0.029987	0.029981	0.029976	0.029977	
	8	0.28735	0.037424	0.037397	0.037389	0.037385	0.037382	0.03738	0.037382	
	9	0.288658	0.046667	0.046654	0.04665	0.046648	0.046647	0.046646	0.046648	
	10	0.29054	0.057368	0.057362	0.057359	0.057358	0.057357	0.057356	0.057361	

The results of the frequency parameters $\Omega_{n,m} = \omega R(\rho(1-\mu^2)/E)^{1/2}$ of the proposed structure obtained based on the theoretical formulation established in Section 2 are shown in Table 3, comparing with those of the literature. The structure used for comparison is a two-stepped cylindrical shell and the geometry are R = 1 m, $h_1 = 0.01 \text{ m}$, $h_2 = 0.005 \text{ m}$, $L_1 = 0.5 \text{ m}$, $L_2 = 0.5 \text{ m}$. As shown in Table 3, the results of the frequency parameters obtained by the proposed method are found to be in very good agreement for all boundary conditions, length to radius ratio and circumferential

wave number. From the comparison results in Tables 1 and 2, it can be seen that the vibration characteristics of the MSCS can be accurately predicted by presented method.

Since the aim of this study is to analyze the vibro-acoustic characteristics of MSCS, it is necessary to verify the accuracy of the sound radiation characteristics by the proposed method.

To verify the accuracy of the current method for sound radiation characteristics, Fig. 3 shows the comparison of the radiation directivity for a uniform cylindrical shell made of steel. The shell is immersed in air, the sound pressures are measured in R_Q = 15 m and R_Q = 30 m. The geometric and material properties of the shell are as follows: L = 2 m, R = 1 m, h = 0.01 m, E = 210 GPa, μ = 0.3, ρ = 7800 kg/m³. The unit surface load 1 N is acted on the normal direction and

location is defined as $x_0 = 0$ m, $x_1 = 0.2$ m, $\theta_0 = -\pi/3$, $\theta_1 = \pi/3$. The excitation frequency due to external force is 100 Hz. From Fig. 3, it is clearly seen that the directivity pattern of radiated sound pressure by the present method is in very good agreement with the results of the previous work.

Table 3 Comparison of frequency parameters $\Omega_{n,m} = \omega R(\rho(1-\mu^2)/E)^{1/2}$ for a two-stepped cylindrical shell $(R=1 \text{ m}, h_1=0.01 \text{ m}, h_2=0.005 \text{ m}, L_1=0.5 \text{ m}, L_2=0.5 \text{ m}, m=1)$.

		C-C C-F				SD-SD							
L/R	n	Ref. [32]	Present	Error,%									
1	1	0.85102	0.850366	0.0768	0.637347	0.637321	0.004	0.549333	0.549335	-0.0003	0.839591	0.839553	0.0045
	2	0.657085	0.65755	-0.0708	0.409449	0.4094	0.0119	0.622456	0.622438	0.0029	0.656497	0.656429	0.0103
	3	0.510742	0.509804	0.1837	0.275042	0.274997	0.0163	0.461383	0.461324	0.0128	0.504898	0.504808	0.0179
	4	0.409108	0.408307	0.1958	0.194546	0.19452	0.0131	0.342895	0.342824	0.0208	0.396288	0.396207	0.0204
	5	0.339613	0.341667	-0.6049	0.147324	0.147309	0.0099	0.265036	0.26501	0.0098	0.321537	0.321406	0.0409
	6	0.294328	0.293368	0.3262	0.123625	0.123493	0.1065	0.220569	0.220305	0.1197	0.273013	0.272898	0.0422
	7	0.269226	0.268295	0.3459	0.118172	0.118098	0.063	0.203862	0.203571	0.1428	0.246394	0.246131	0.1069
	8	0.26175	0.260729	0.3901	0.126063	0.125925	0.1092	0.208817	0.208586	0.1104	0.238499	0.238227	0.1141
5	1	0.236939	0.236938	0.0002	0.097836	0.097834	0.0025	0.17659	0.17659	7E-05	0.221194	0.221191	0.0012
	2	0.124523	0.124523	0.0001	0.037807	0.037803	0.0109	0.072988	0.072999	-0.0155	0.1057	0.105691	0.0086
	3	0.073567	0.073626	-0.0805	0.022411	0.022388	0.101	0.041159	0.041145	0.0344	0.059344	0.059324	0.0343
	4	0.057271	0.057203	0.1189	0.025746	0.025715	0.1222	0.041561	0.041498	0.1519	0.047681	0.047643	0.0794
	5	0.062517	0.062521	-0.0066	0.036509	0.036506	0.0095	0.053819	0.053735	0.1559	0.054198	0.054207	-0.016
	6	0.072523	0.072498	0.0347	0.051206	0.051197	0.0175	0.064339	0.064284	0.0848	0.064347	0.064329	0.0274
	7	0.083824	0.083803	0.0256	0.069402	0.069386	0.0225	0.07795	0.077932	0.0236	0.077951	0.077929	0.0282
	8	0.100175	0.100131	0.0443	0.090757	0.090731	0.0289	0.09646	0.096436	0.0245	0.09646	0.09643	0.031
10	1	0.097703	0.097713	-0.0106	0.029471	0.029473	-0.006	0.056538	0.056537	0.0016	0.082455	0.082459	-0.005
	2	0.041392	0.041359	0.0805	0.010877	0.010885	-0.07	0.02075	0.020806	-0.2698	0.032011	0.032002	0.0288
	3	0.027756	0.027767	-0.0407	0.012918	0.012923	-0.037	0.020546	0.020455	0.4449	0.02286	0.022912	-0.226
	4	0.033748	0.033723	0.0738	0.021782	0.02178	0.0075	0.029146	0.029155	-0.0295	0.029148	0.029109	0.1344
	5	0.041385	0.041375	0.0247	0.034298	0.034297	0.0041	0.038195	0.038188	0.0196	0.038196	0.038195	0.0033
	6	0.053611	0.0536	0.0212	0.049998	0.049996	0.0045	0.052	0.051992	0.0163	0.052	0.051992	0.0151
	7	0.070682	0.070674	0.011	0.068678	0.068669	0.0131	0.069888	0.069872	0.0222	0.069888	0.069873	0.0221
	8	0.091582	0.091556	0.028	0.090272	0.090253	0.0206	0.091165	0.091139	0.0288	0.091165	0.091139	0.0288

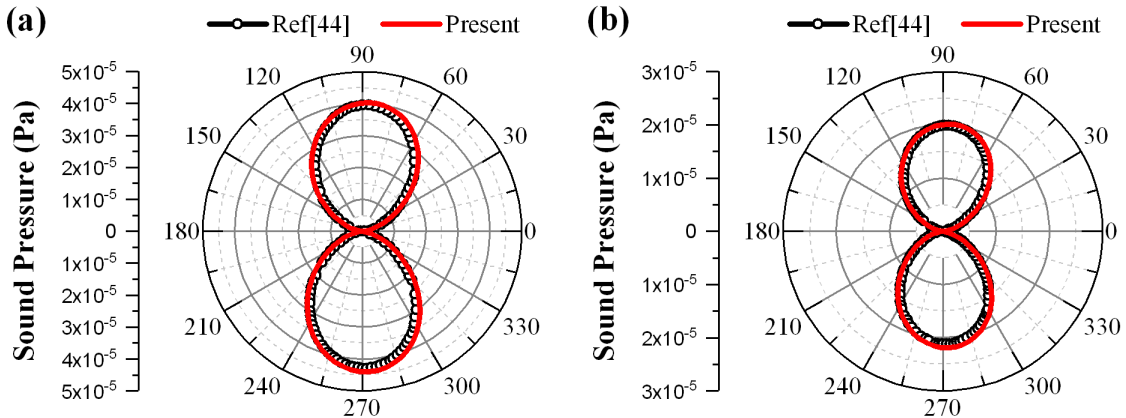


Fig. 3 Comparison of the directivity pattern of radiated sound pressure for uniform cylindrical shell: (a) $R_0 = 15$ m; (b) $R_0 = 30$ m.

Then, the sound pressure level and sound power level results of the uniform cylindrical shell and MSCS made of steel obtained by presented method are compared with the results of FEM/BEM, and the comparison results are shown in Fig. 4. The material properties of both the uniform cylindrical shell and MSCS are E = 210 GPa, $\mu = 0.3$, $\rho = 7800$ kg/m³. And the geometric dimensions are as follows: L = 4 m, R = 1 m, h = 0.05 m for uniform cylindrical shell; $L_1 = 1$ m, $L_2 = 1$ m, $L_3 = 1$ m, R = 1 m

= 0.5 m, θ = 0 for MSCS. The excitation frequencies due to external force are 250 Hz and 200 Hz for uniform shell and MSCS, respectively. The sound radiation characteristics of the shells are measured in R_Q = 5 m, and C-C boundary condition is considered.

As shown in Fig. 4, the results of sound radiation characteristics by the proposed method for both kinds of shells are in very good agreement with those of the FEM/BEM, and it can be concluded that the present method is an accurate and effective method for the analysis of the acoustic characteristics of the MSCS.

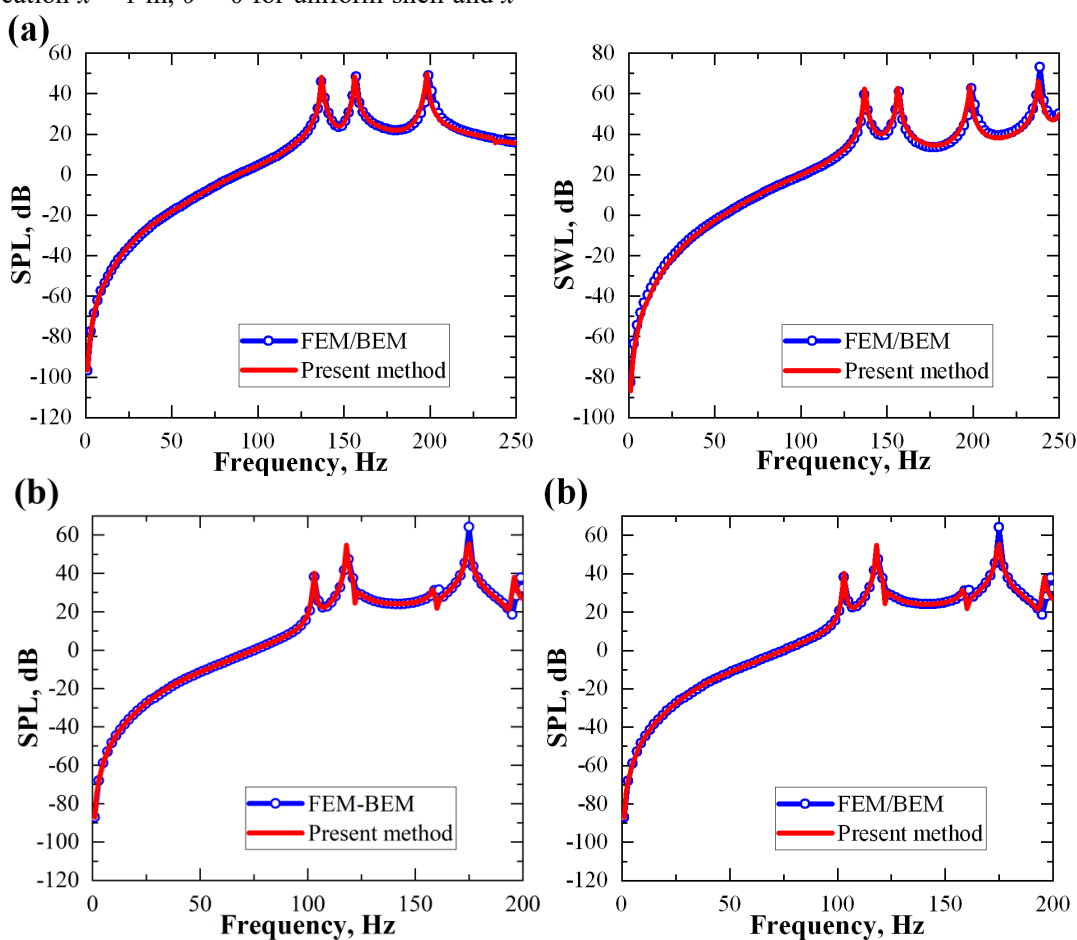


Fig. 4 Comparison of sound radiation results of a uniform cylindrical shell (a) and a MSCS (b).

3.2 Sound Radiation Characteristics

By combining different geometric dimensions such as thickness, length, and radius, many types of stepped shells can be obtained. Since it is impossible to perform the analysis for all the possible combinations of step shells, in this work, the acoustic analysis of the following four types of step shells are performed.

Case I: two-stepped shell; $L_1 = 1$ m, $L_1:L_2 = 1:2$, $h_1 = 0.01$ m, $h_1:h_2 = 1:2$

Case II: three-stepped shell; $L_1 = 1$ m, $L_1:L_2:L_3 =$

1:1:1; $h_1 = 0.01$ m, $h_1:h_2:h_3 = 1:2:1$

Case III: three-stepped shell; $L_1 = 1$ m, $L_1:L_2:L_3 = 1:2:1$; $h_1 = 0.01$ m, $h_1:h_2:h_3 = 1:2:1$

Case IV: five-stepped shell; $L_1 = 1$ m, $L_1:L_2:L_3:L_4:L_5 = 1:1:1:1:1$, $h_1 = 0.01$ m, $h_1:h_2:h_3:h_4:h_5 = 1:2:1:2:1$.

In addition, in all the numerical examples below, the material properties of the MSCS are assumed to be E = 210 GPa, $\mu = 0.3$, $\rho = 7800$ kg/m³. Fig. 5 shows the sound radiation characteristics of the MSCS under

different classical and elastic boundary conditions. Two kinds of classical boundary conditions (C-C and C-F) and one elastic boundary condition (E_1 - E_1) are considered. For all boundary conditions and shells, it is assumed that the unit point load 1N is acted on the location x=0.5 m, $\theta=0$, and the excitation frequencies due to external force are set 200 Hz. The sound radiation characteristics of the MSCS are measured in $R_O=5$ m for all cases.

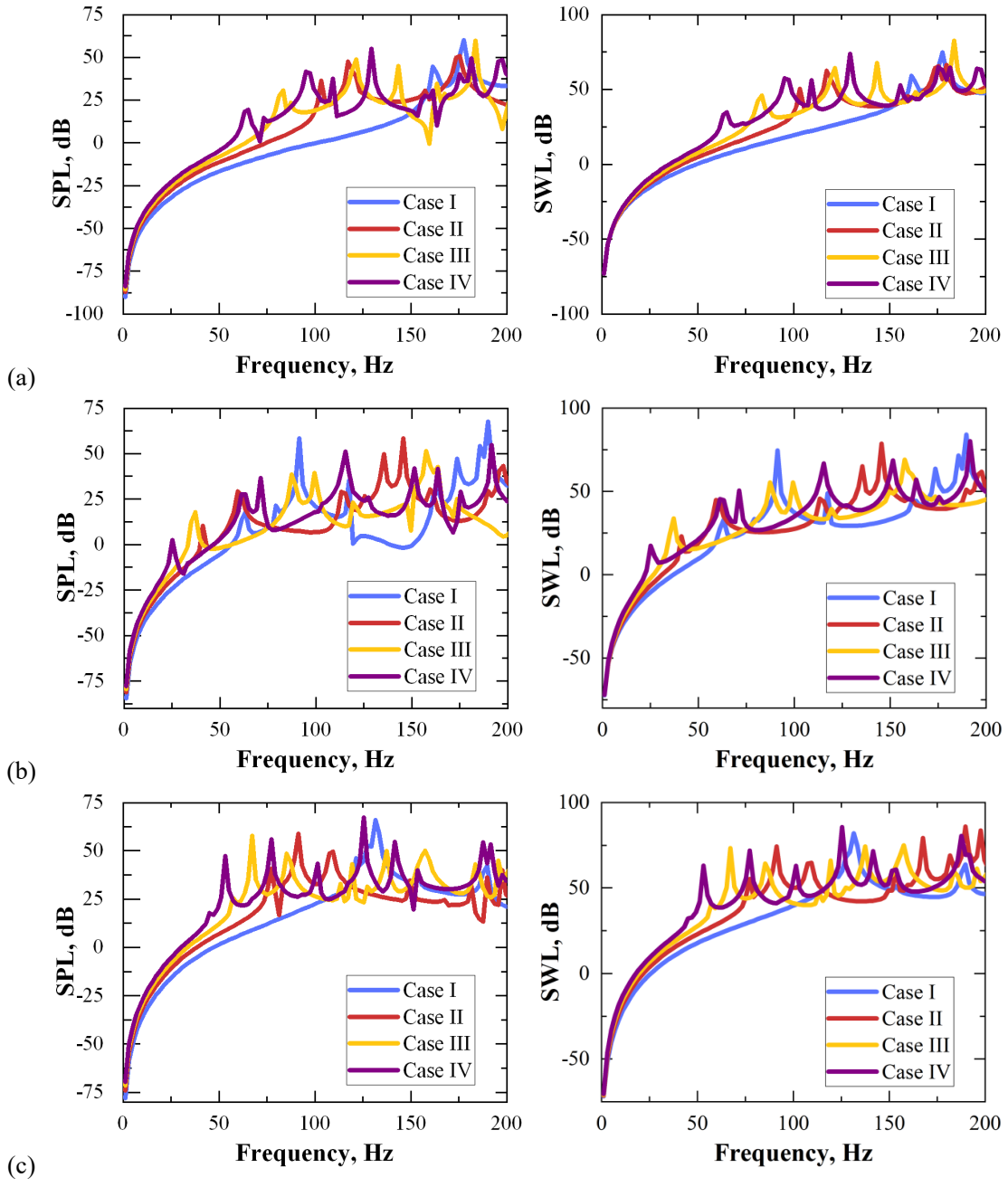


Fig. 5 Radiated sound characteristics results of MSCS with different boundary conditions; (a): C-C, (b): C-F, (c): E₁-E₁.

As shown in Fig. 5, the change of boundary conditions leads to the change of the sound radiation characteristics of the MSCS. Thus, the sound radiation characteristics of MSCS are different depending on the different boundary conditions. In particular, it can be seen that the change of the sound radiation characteristics in the case of the C-F boundary condition is more pronounced than the other boundary conditions.

The reason may be related to the high frequency variation in the case of C-F boundary conditions in the specified frequency range.

Next, the effect of the applied load type on the sound radiation characteristics of MSCS is investigated. The location of the force is x = 0.5 m, $\theta = 0$ for the point force, $x_0 = 0.2$, $x_1 = 0.8$ m, $\theta = 0$ for the line force, $x_0 = 0.2$ m, $x_1 = 0.8$ m, $\theta_0 = -\pi/3$, $\theta_1 = \pi/3$ for the surface force. The sound radiation

characteristics of the MSCS are measured in $R_Q = 5$ m, and elastic boundary condition E_1 - E_3 is considered. Fig. 6 shows the radiated sound characteristics of MSCS for different applied force types.

As can be seen in Fig. 6, the sound radiation characteristics of the MSCS are clearly different depending on the type of applied load. This is because the pressure is different according to the applied area when the same unit load is applied, thus, the displacement characteristics result is changed. As can be seen in Fig. 6, the results of sound radiation for point force are the largest and the lowest for surface force. Interestingly, in this study, both cases considered are three-stepped cylindrical shells. Although both shells are three-stepped shells, the shape of the shells varies with length and thickness, and thus, the sound radiation characteristics of are also different.

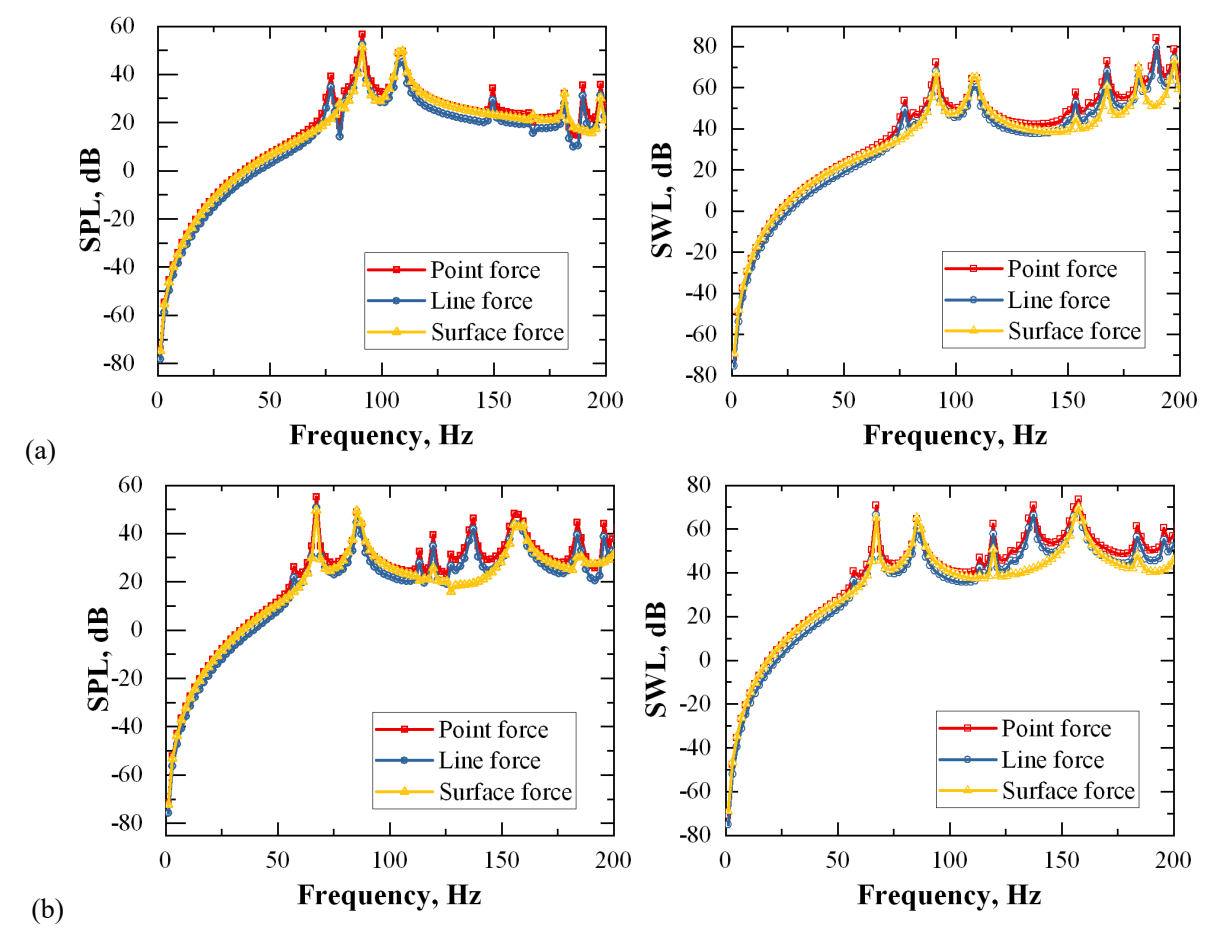


Fig. 6 Radiated sound characteristics of MSCS for different applied force types; (a): Case II, (b): Case III.

Fig. 7 shows the grouped modal contributions of the circumferential modes to the sound radiation of MSCS. Case IV shell with C-C boundary condition is considered. From Fig. 7, the contribution of different circumferential modes to the sound radiation is different. And when n > 6, the higher-order

circumferential modes have almost no effects on radiated sound results within the frequency range considered. However, it should be emphasized here, its influence range will appear in a higher frequency band.

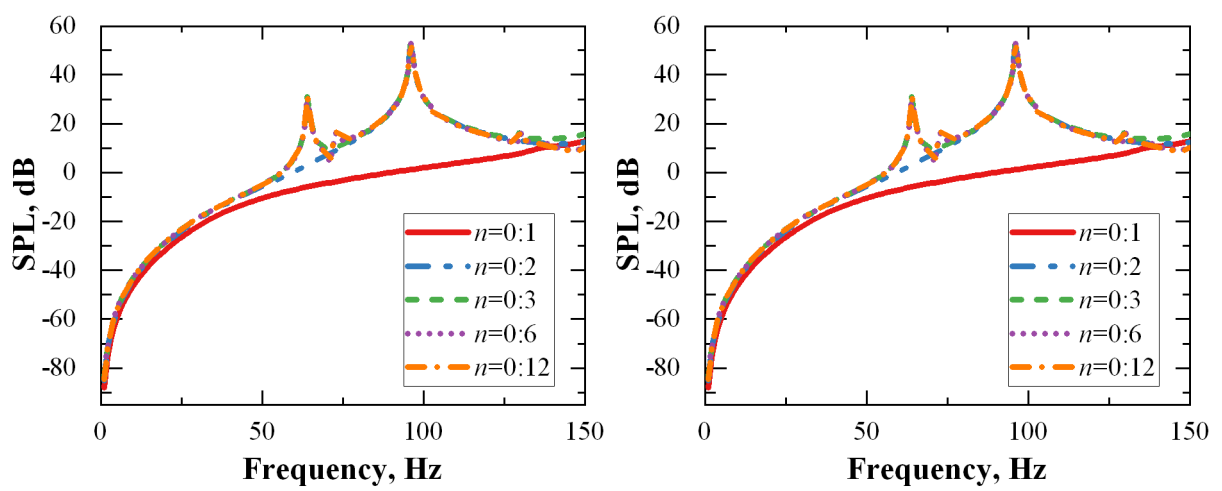


Fig. 7 Radiated sound results of MSCS (Case IV) with different circumferential modes.

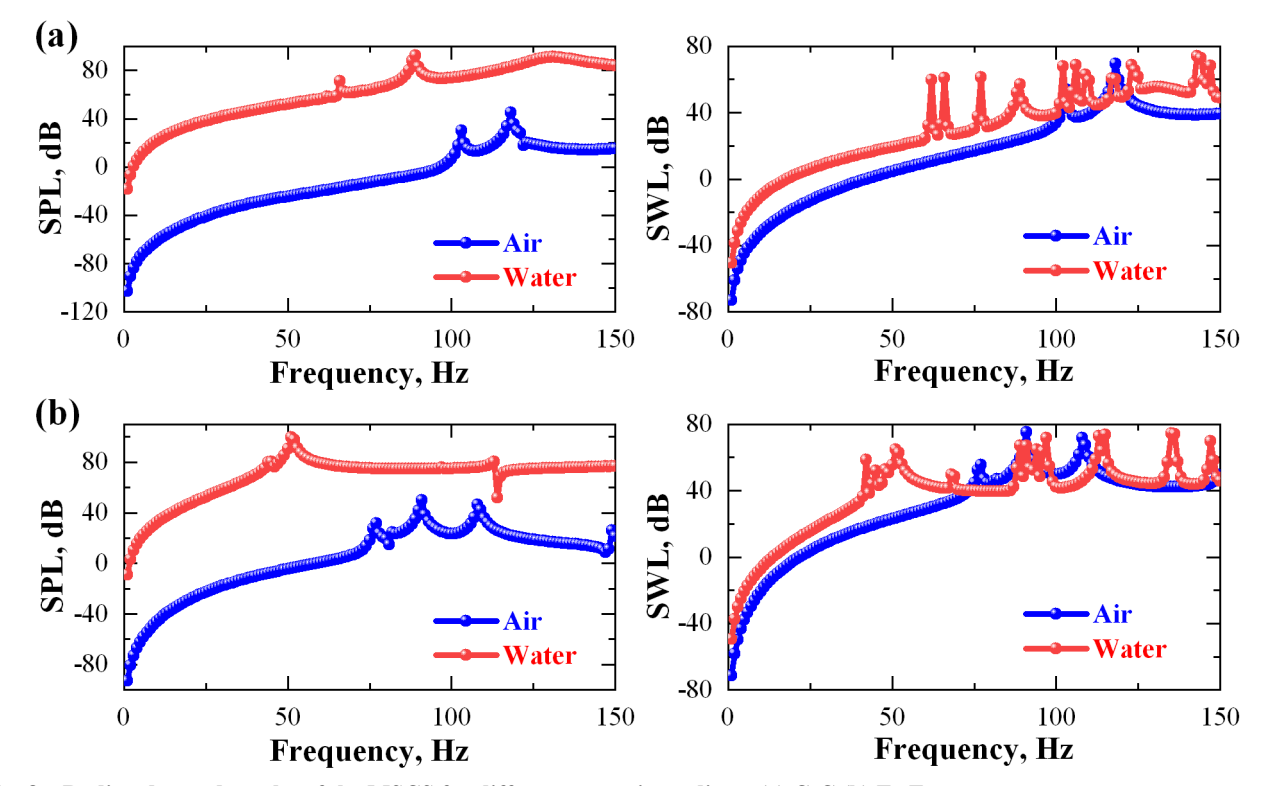


Fig. 8 Radiated sound results of the MSCS for different acoustic medium; (a) C-C (b) E₃-E₃.

Fig. 8 shows the radiated sound results of MSCS immersed in different acoustic medium: air and water.

The sound radiation characteristics of the MSCS are measured in $R_Q = 15$ m, and Case II shells with C-C

and E_3 - E_3 boundary condition are considered. It is assumed that the unit point load 1N is acted on the location x = 0.5 m, $\theta = 0$ in normal direction, and the excitation frequencies due to external force are set 150 Hz. As can be seen from Fig. 8, the properties of acoustic medium have an important influence on the sound radiation characteristic of the MSCS. The

radiated sound results of water (heavy medium) is higher than that of air (light medium).

Then, Fig. 9 and Fig. 10 shows circumferential directivity plots of the Case II MSCS immersed in air and water. The clamped boundary condition is considered. It is assumed that the unit point load 1 N is acted on the location x = 1.5 m, $\theta = 0$ in normal

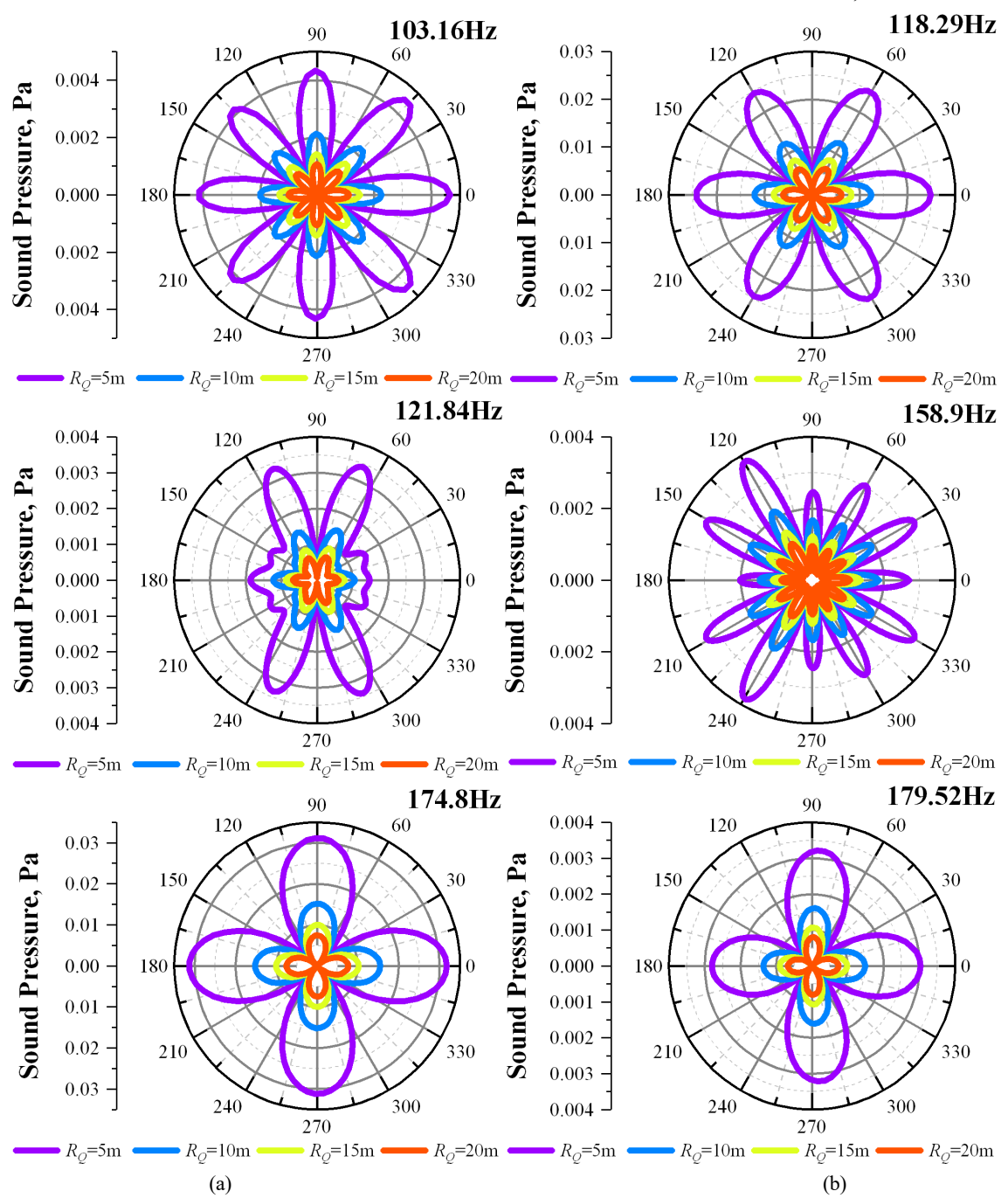


Fig. 9 Circumferential directivity plots of radiated sound pressure for MSCS immersed in air.

direction. These directivity plots are obtained at first six frequencies, i.e., 103.16 Hz, 118.29 Hz, 121.84 Hz, 158.9 Hz, 174.8 Hz and 179.52 Hz. In the circumferential directivity plots four kinds of

circumferential distances are taken into account, i.e., R_Q = 5 m, R_Q = 10 m, R_Q = 15 m and R_Q = 20 m for Fig. 9 and R_Q = 5 m, R_Q = 6 m, R_Q = 7 m and R_Q = 8 m for Fig. 10.

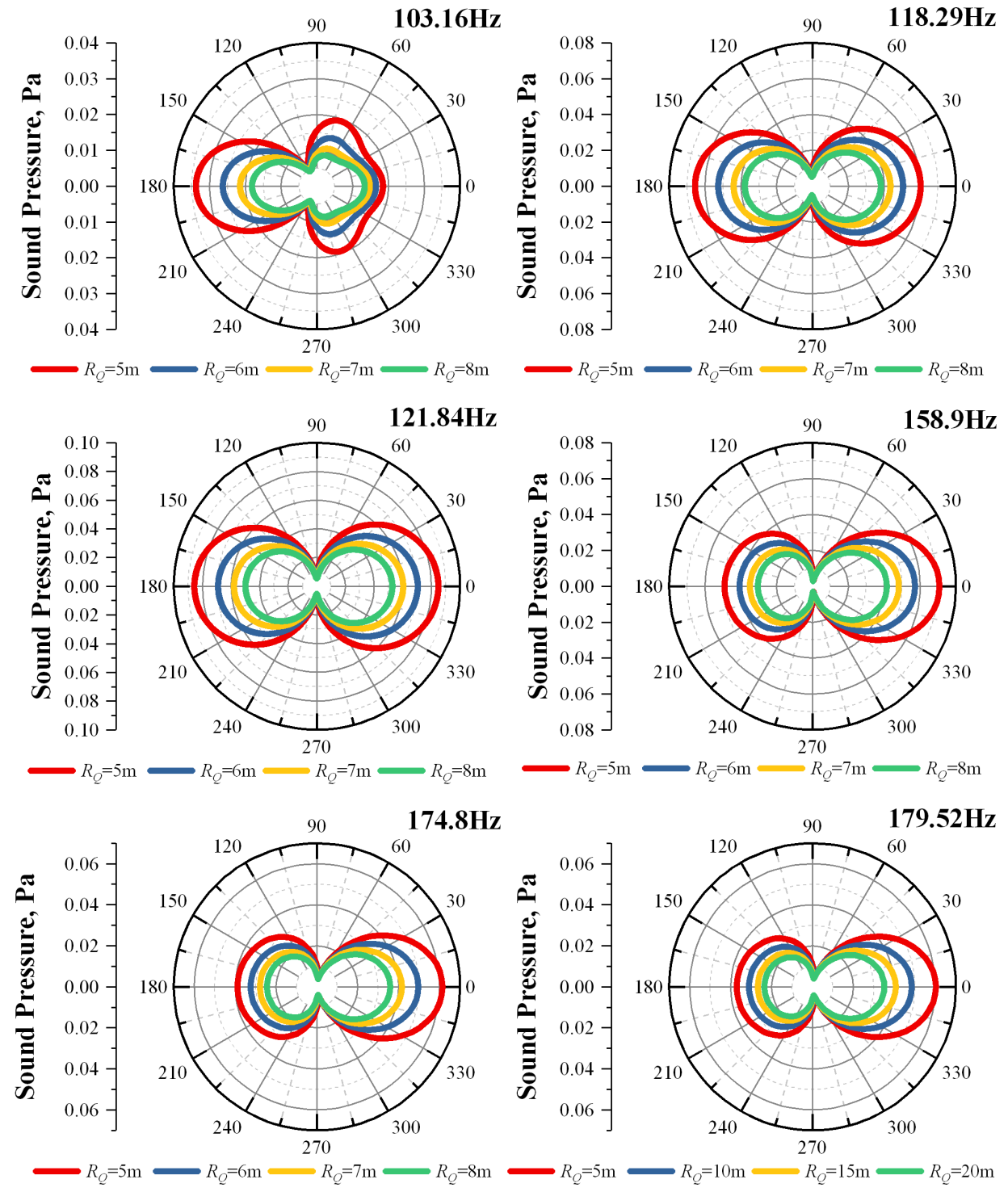


Fig. 10 Circumferential directivity plots of radiated sound pressure for MSCS immersed in water.

As shown in Fig. 9, the intensity of sound pressure decreases rapidly with increasing distance from the measurement location. This phenomenon can be attributed to the physical properties of acoustic

medium. To improve the reader's understanding of the sound radiation characteristics, Fig. 11 shows the sound pressure contours of the MSCS immersed in air corresponding to the first six frequencies.

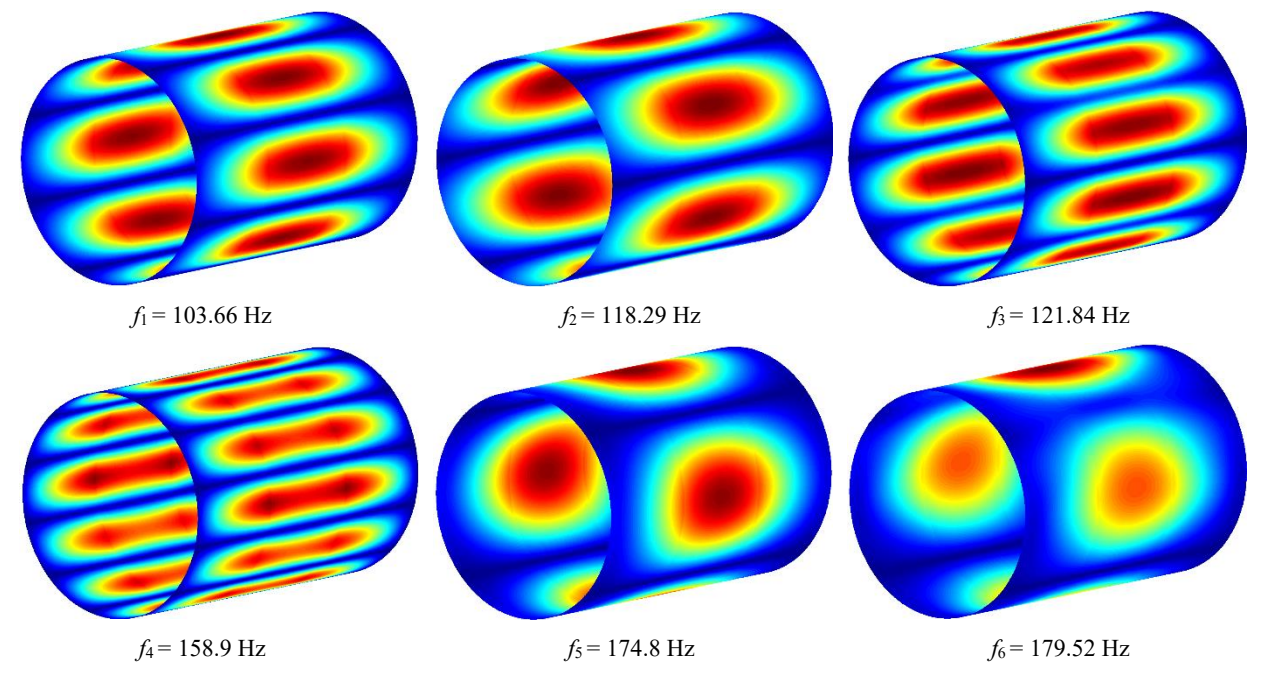


Fig. 11 Sound pressure contours of MSCS immersed in air.

4. Conclusion

This paper is investigated the vibro-acoustic characteristics of (MSCS) immersed in infinite fluid medium by using a semi-analytical method. Based on the Flugge's thin shell theory, the theoretical model for vibro-acoustic analysis of the MSCS is formulated by using the energy method and spectral boundary element method. The variables describing the displacement and acoustic properties of the structure are expressed as Chebyshev orthogonal polynomials in the meridional direction and Fourier series in the circumferential direction. The external acoustic field of the MSCS is formulated by the spectral Helmholtz integral equation with the collocation points. The non-uniqueness solution of the acoustic integral equation is solved using the CHIEF method. Comparison studies are performed to verify the accuracy, convergence and reliability of the proposed method. Finally, the vibro-acoustic responses of MSCS immersed in fluid medium with various geometries, material properties and boundary conditions are investigated through numerical examples.

Acknowledgement

The authors would like to take the opportunity to express my hearted gratitude to all those who made contributions to the completion of my article.

References

- [1] Quta, M. S. (2004). *Vibration of Laminated Shells and Plates*, San Diego: Elsevier.
- [2] Jin, G., Ye, T., & Su, Z. (2015). Structural Vibration: A Uniform Accurate Solution for Laminated Beams, Plates and Shells With General Boundary Conditions, Science Press, Springer, Beijing
- [3] Qu, Y. G., Hua, H. X., & Meng G. (2013). A domain decomposition approach for vibration analysis of isotropic and composite cylindrical shells with arbitrary boundaries, *Compos. Struct.*, 95: 307-321.

- [4] Qu, Y. G., Long, X. H., Wu, S. H., & Meng, G. (2013). A unified formulation for vibration analysis of composite laminated shells of revolution including shear deformation and rotary inertia, *Compos. Struct.*, 98: 169-191.
- [5] He, D. et al. (2019). Wave based method (WBM) for free vibration analysis of cross-ply composite laminated cylindrical shells with arbitrary boundaries, *Compos.* Struct., 213: 284-298.
- [6] Shi, D. et al. (2019). Wave based method for free vibration analysis of cross-ply composite laminated shallow shells with general boundary conditions, *Materials*, 12: 3808.
- [7] Dongyan, S. et al. (2020). Free vibration analysis of closed moderately thick cross-ply composite laminated cylindrical shell with arbitrary boundary conditions, *Materials*, 13: 884, doi: https://doi.org/0.3390/ma13040884.
- [8] Dongze, H. et al. (2021). A unified power series method for vibration analysis of composite laminate conical, cylindrical shell and annular plate, *Structures*, 29: 305-327.
- [9] Zhao, X., Ng, T. Y., & Liew, K. M. (2004). Free vibration of two-side simply-supported laminated cylindrical panels via the mesh-free kp-Ritz method, *Int J. Mech Sci.*, 46: 123-142.
- [10] Haftchenari, H, Darvizeh, M, Darvizeh A, Ansari R, & Sharma C. B. (2007). Dynamic analysis of composite cylindrical shells using differential quadrature method (DQM), Compos Struct., 78: 292-298.
- [11] Alibeigloo, A. (2009). Static and vibration analysis of axi-symmetric angle-ply laminated cylindrical shell using state space differential quadrature method, *Int J. Press Vessels Pip*, 86: 738-747.
- [12] Malekzadeh, P., Farid, M., & Zahedinejad, P. (2008). A three-dimensional layerwise-differential quadrature free vibration analysis of laminated cylindrical shells, *Int J. Press Vessels Pip*, 85: 450-458.
- [13] Tornabene, F., Viola, E., & Inman, D. J. (2009). 2-D differential quadrature solution for vibration analysis of functionally graded conical, cylindrical shell and annular plate structures, *J. Sound Vib.*, 328 (3): 259-290.
- [14] Carrera, E. (2002). Theories and fnite elements for multilayered, anisotropic, composite plates and shells, *Arch Comput Methods Eng.*, *9*: 87-140.
- [15] Mohammadi, F., & Sedaghati, R. (2012). Vibration analysis and design optimization of viscoelastic sandwich cylindrical shell, J. Sound Vib., 331: 2729-2752.
- [16] Chakravorty, D., Bandyopadhyay, J. N., & Sinha, P. K. (1995). Finite element free vibration analysis of point supported laminated composite cylindrical shells, *J. Sound Vib.*, 181 (1): 43-52.

- [17] Zhang, X. M. (2001). Vibration analysis of cross-ply laminated composite cylindrical shells using the wave propagation approach, *Appl. Acoust.*, 62 (11): 1221-1228.
- [18] Zhang, X. M. (2002). Parametric analysis of frequency of rotating laminated composite cylindrical shells with the wave propagation approach, *Comput. Method Appl. Mech.*, 191: 2029-2043.
- [19] Haddadpour, H, Mahmoudkhani, S, & Navazi, H. M. (2007). Free vibration analysis of functionally graded cylindrical shells including thermal effects, *Thin-Walled Struct.*, 45: 591-599.
- [20] Lam, K. Y., & Loy, C. T. (1998). Influence of boundary conditions for a thin laminated rotating cylindrical shell, *Compos Struct.*, 41: 215-228.
- [21] Liew, K. M., Ng, T. Y., Zhao, X., & Reddy, J. N. (2002). Harmonic reproducing kernel particle method for free vibration analysis of rotating cylindrical shells, *Comput. Method Appl. Mech. Eng.*, 191: 4141-4157.
- [22] Songhun, K. et al. (2020). Natural frequency calculation of open laminated conical and cylindrical shells by a meshless method, *Eur. Phys. J. Plus*, 135: 434, doi: https://doi.org/10.1140/epjp/s13360-020-00438-0.
- [23] Songhun, K. et al. (2021). A novel meshfree method for three-dimensional natural frequency analysis of thick laminated conical, cylindrical shells and annular plates, *Phys. Scr.*, 96: 125204, doi: https://doi.org/10.1088/1402-4896/ac1a8b
- [24] Thinh, T. I., & Nguyen, M. C. (2013). Dynamic stiffness matrix of continuous element for vibration of thick cross-ply laminated composite cylindrical shells, *Compos Struct.*, 98: 93-102.
- [25] Xudong, C., & Kangsheng, Y. (2016). Comparison study on the exact dynamic stiffness method for free vibration of thin and moderately thick circular cylindrical shells, *Shock and Vibration*, 9748135: 14, doi: http://dx.doi.org/10.1155/2016/9748135
- [26] El-Kaabazi, N., & Kennedy, D. (2012). Calculation of natural frequencies and vibration modes of variable thickness cylindrical shells using the Wittrick-Williams algorithm, *Computers and Structures*, 104-105: 4-12.
- [27] Civalek, Ö. (2007). Numerical analysis of free vibrations of laminated composite conical and cylindrical shells: Discrete singular convolution (DSC) approach, *J. Comput. Appl. Math*, 205 (1): 251-271.
- [28] Civalek, Ö. (2013). Vibration analysis of laminated composite conical shells by the method of discrete singular convolution based on the shear deformation theory, *Compos Part B: Eng.*, 45: 1001-1009.
- [29] Xiang, X. et al. 2014. Free vibration analysis of composite laminated cylindrical shells using the Haar wavelet method, *Compos. Struct.*, 109: 169-177.

- [30] Xiang, X. et al. (2014). A numerical solution for vibration analysis of composite laminated conical, cylindrical shell and annular plate structures, *Compos Struct.*, 111: 20-30.
- [31] Zhang, L., & Xiang, Y. (2007). Exact solutions for vibration of stepped circular cylindrical shells, *J. Sound Vib.*, 299: 948-964.
- [32] Haichao, L. et al. (2019). Jacobi-Ritz method for free vibration analysis of uniform and stepped circular cylindrical shells with arbitrary boundary conditions: A unified formulation, *Comput. Math Appl.*, 77: 427-440.
- [33] Qu, Y. et al. (2013). Free and forced vibration analysis of uniform and stepped circular cylindrical shells using a domain decomposition method, *Appl. Acoust.*, 74: 425-439.
- [34] Jeans, R. A., & Mathews, I. C. (1990). Solution of fluid-structure interaction problems using a coupled finite element and variational boundary element technique, *J. Acoust. Soc. Am.*, 88 (5): 2459-2466.
- [35] Everstine, G. C., & Henderson, F. M. (1990). Coupled finite element/boundary element approach for fluid-structure interaction, *J. Acoust. Soc. Am.*, 87: 1938-1947.
- [36] Chen, S., & Liu, Y. (1999). A unified boundary element method for the analysis of sound and shell-like structure interactions: I. Formulation and verification. *J. Acoust. Soc. Am.*, 106 (3): 1247-1254.
- [37] Caresta, M., & Kessissoglou, N. J. (2009). Structural and acoustic responses of a fluid-loaded cylindrical hull with structural discontinuities, *Appl. Acoust.*, 70: 954-963.
- [38] Peters, H., Kessissoglou, N., & Marburg, S. (2013). Modal decomposition of exterior acoustic-structure interaction problems with model order reduction, *J. Acoust. Soc. Am.*, 133: 2706-2717.
- [39] Peters. H., Kinns, R., & Kessissoglou, N. J. (2014). Effects of internal mass distribution and its isolation on the acoustic characteristics of a submerged hull, *J. Sound Vib.*, 333 (6): 1684-1697.
- [40] Denli, H., & Sun, J. Q. (2008). Structural-acoustic optimization of sandwich cylindrical shells for minimum interior sound transmission, *J. Sound Vib.*, 316 (1-5): 32-49.
- [41] Bérot, F., & Peseux, B. (1998). Vibro-acoustic behavior of submerged cylindrical shells: Analytical formulation and numerical model, *J. Fluids Struct.*, 12: 959-1003.
- [42] Caresta, M., & Kessissoglou, N. J. (2010). Acoustic signature of a submarine hull under harmonic excitation, *Appl. Acoust.*, 71: 17-31.
- [43] Caresta, M. et al. (2008). Low frequency structural and acoustic responses of a submarine hull, *Acoust. Australia*, 36: 47-52.

- [44] Chen, L., Liang, X., & Yi, H. (2016). Vibro-acoustic characteristics of cylindrical shells with complex acoustic boundary conditions, *Ocean Eng.*, *126*: 12-21.
- [45] Qu, Y. et al. (2015). Vibro-acoustic analysis of multilayered shells of revolution based on a general higher-order shear deformable zig-zag theory, *Compos Struct.*, 134: 689-707.
- [46] Zou, M. S., Liu, S. X., & Qi, L. B. (2019). An analytical formulation for the underwater acoustic radiation of a cylindrical shell with an internal flexural floor based on the reciprocity theorem, *Appl. Acoust.*, 154: 18-27.
- [47] Liu, S. X. et al. (2018). Vibratory response and acoustic radiation of a finite cylindrical shell partially covered with circumferential compliant layers, *Appl. Acoust.*, 141: 188-197.
- [48] Wang, X. et al. (2018). Experiment and modeling of vibro-acoustic response of a stiffened submerged cylindrical shell with force and acoustic excitation, *Results Phys.*, 11: 315-324.
- [49] Ciskowski, R. D., & Brebbia, C. A. (1991). Boundary element methods in acoustics, Southampton: Computational Mechanics Publications.
- [50] Schenck, H. A. 1968. Improved integral formulation for acoustic radiation problems, J. Acoust Soc. Am., 44: 41-58.
- [51] Burton, A. J., & Miller, G. F. (1971). The application of integral equation methods to the numerical solution of some exterior boundary-value problems, *Proc. R. Soc. A.*: *Math Phys. Eng. Sci.*, 323 (1553): 201-210.
- [52] Qu, Y., Hua, H., & Meng, G. (2015). Vibro-acoustic analysis of coupled spherical-cylindrical-spherical shells stiffened by ring and stringer reinforcements, *J. Sound Vib.*, 355: 345-359.
- [53] Qu, Y., & Meng, G. (2016). Prediction of acoustic radiation from functionally graded shells of revolution in light and heavy fluids, *J. Sound Vib.*, *376*: 112-130.
- [54] Wang, X., & Guo, W. (2016). Dynamic modeling and vibration characteristics analysis of submerged stiffened combined shells, *Ocean Eng.*, 127: 226-235.
- [55] Xie, K. et al. (2019). "A unified semi-analytic method for vibro-acoustic analysis of submerged shells of revolution", *Ocean Eng.*, 189: 106345.
- [56] Jin, G. et al. (2018). An energy-based formulation for vibro-acoustic analysis of submerged submarine hull structures, *Ocean Eng.*, 164: 402-413.
- [57] Guan, X. et al. (2021). Vibro-acoustic analysis of combined elliptical-cylindrical-elliptical shells immersed in acoustic medium, *J. Fluids Struct*, 106: 103391, doi: https://doi.org/10.1016/j.jfluidstructs.2021.103391.